Origin of Red Emission in β-Ga_2O_3 Analysed by Cathodoluminescence and Photoluminescence Spectroscopy

G. Naresh-Kumar[1*], H. Macintyre[1], S. Shanthi[2], P. R. Edwards[1], R.W. Martin[1], D. Krishnamurthy[3], K. Sasaki[3], and A. Kuramata[3]

[1] *Department of Physics, SUPA, University of Strathclyde, Glasgow G4 0NG, UK*

[2] *Crystal growth centre, Anna University, 600 0025, India*

[3] *Novel Crystal Technology, Hirosedai, Saitama prefecture, Saitama city, 350-1328, Japan*

E-mail: naresh.gunasekar@strath.ac.uk

Keywords: Gallium oxide, un-intentional doping cathodoluminescence and photoluminescence spectroscopy.

Abstract

The spectroscopic techniques of cathodoluminescence and photoluminescence are used to study the origin of red emission in β-Ga_2O_3 grown using the edge-defined film-fed grown (EFG) method and hydride vapor phase epitaxy. Room temperature cathodoluminescence shows red emission peaks from samples doped with Fe, Sn, and Si and from unintentionally doped samples. Narrow emission lines around 690 nm are seen strongly in the Fe and unintentionally doped samples. Temperature-dependent photoluminescence analysis of the two prominent red emission lines reveals properties similar to the R lines in sapphire for all the samples, but with different level of existence. These lines are attributed to Cr^{3+} ionic transitions rather than to Fe^{3+}, as reported previously. The most likely origin of the unintentional Cr incorporation is the source material used in the EFG method.

1. Introduction

Two figures of merit, the Baliga figure of merit (BFOM) and Huang's material figure of merit (HMFOM), are often used to assess the suitability of a material and rank its performance for power electronics applications. The BFOM estimates the direct current (DC) conduction losses and HMFOM estimates the dynamic switching losses . Both include the breakdown field, which

is dependent on the bandgap of a semiconductor. Larger bandgaps allow the material to withstand a stronger electric field, making it possible to produce ultrathin devices for a given voltage. Thinner devices can have lower resistance and thus higher efficiency. Monoclinic β - Ga_2O_3 has attracted massive interest in power electronics device applications due to its ultra-wide bandgap in the range of 4.6- 4.9 eV with a large breakdown field of ≈ 8 MVcm $^{-1}$ and a BFOM three times larger than GaN and ten times larger than 4H-SiC and a HMFOM of similar order as GaN [1]. The recent record for a Ga_2O_3 metal oxide field-effect transistor (MOSFET) device breakdown voltage of 1.8 kV with a power figure of merit of 155 MW/cm ^{2}, demonstrate its great potential as a future power electronics device material that could overtake SiC and GaN [2,3]. In addition to the larger bandgap, the transmission of ≈ 90% of visible light makes Ga_2O_3 a leading contender for UV optoelectronics applications such as solar-blind photodetectors and scintillators [4,5]. All these applications require control of charge carrier densities by controlled incorporation of various dopants using a variety of growth methods. The knowledge and position of electronic states due to the different dopants is critical for electronic device operation and reliability.

The control of doping in Ga_2O_3 is complicated due to self-compensation and defect issues, particularly due to point defects. Study of the light emission, and thereby the associated electronic transitions, provides an understanding of the presence of point defects and their impact on optical and electrical properties. The optical properties of β - Ga_2O_3 grown by various methods with different dopants have been widely reported [5-9], primarily for emission in the UV and blue regions of the visible spectrum. However, there are only few reports [10-14] on emission in the red spectral region due to transition metals, which is the focus of this work. We discuss red emission in relation to various dopants in β-Ga_2O_3. The optical spectroscopy techniques of cathodoluminescence (CL) and photoluminescence (PL) were employed to gain understanding the possible defect states responsible for specific red emission peaks observed for β - Ga_2O_3 samples with different types of doping.

2. Experimental Section

This study investigates un-intentionally doped (UID), Fe-doped and Sn-doped [010] β - Ga_2O_3 grown by edge-defined film-fed grown (EFG) method [15] as well as Si-doped [010] β - Ga_2O_3 grown by hydride vapour phase epitaxy (HVPE) [16] on Sn-doped EFG β - Ga_2O_3 substrate. Details of the EFG and HVPE growth methods for β - Ga_2O_3 have been reported elsewhere [5,15]. Crucial details required here are the estimated carrier concentration and the unintentional dopants and impurity levels in these samples. Carrier concentrations were measured using capacitance-voltage measurements, giving n-type carrier concentrations of 5.8×10^{18} $cm^{-3,}$ 7×10^{18} $cm^{-3,}$ and 1.3×10^{17} cm^{-3}, for the Sn, Si and Fe doped samples respectively. The carrier concentration measured for the UID sample is 2.4×10^{17} cm^{-3}. The impurity content is measured by secondary ion mass spectrometry (SIMS) where the main impurities in the EFG samples are Si, Fe and Ir. However, Cr and Al were also present [15]. Impurities such as Si, Cr are from the source material (gallium oxide powder), whereas Ir comes mostly from the growth crucible. Also, the annealing gas, e.g. nitrogen, can cause background contamination, including by carbon and hydrogen. The SIMS data for the EFG samples in this study show that in the surface regions of the UID β - Ga_2O_3 sample the concentrations of Fe, Cr, Al, Si and Ir in wt ppm are at 0.81, 0.27,0.81, 2.3 and 4.9 respectively [15].

Room temperature CL is performed in an FEI Quanta 250 Schottky variable pressure FEG–SEM using a custom-built CL system. A Cassegrain reflecting objective is used to collect the emitted light, which is dispersed with a 1/8 m focal length spectrometer (Oriel MS125) onto a 1600-channel electron-multiplying charge-coupled device (Andor Newton). The CL is excited by an electron beam energy of 5 keV. Details of the design of the CL system and its collection optics are given in reference [17]. The CL spectra were obtained using a 400 lines/mm grating and a dwell time of 10 seconds. The CL spectra for the Fe doped sample were recorded in low

vacuum mode since the sample was charging under the electron beam. Low-temperature PL spectroscopy is performed using a custom-built PL system with a closed cycle He cryostat and a 355nm CW laser (Cobolt Zouk) with a maximum power of 20mW as the excitation source. The light emitted from the sample was collected into a 0.67m spectrometer (McPherson 207) with a diffraction grating with 300 lines/mm and dispersed over a cooled CCD (Andor Technology) where each spectrum is collected for 10 seconds. A detailed description of the PL system and the collection optics is given in reference [18].

3. Results and discussion

Figure 1a shows the room temperature CL for all the four samples measured in the region around 500 nm, revealing two strong, broad emission peaks in the UV (373 nm) and blue region (485 nm) and weak, narrow peaks in the near-infrared region (680 – 720 nm), especially for the Fe-doped and UID samples. The broad UV emission is intrinsic, and is widely attributed to the recombination of free electrons and self-trapped holes (STH) [6, 7] or the recombination of free electrons with self-trapped excitons (STE). Generally, STEs are usually observed in alkali halide crystals; however, they have also been observed in β -Ga_2O_3 [8]. The β - Ga_2O_3 unit cell consists of two distinct Ga sites, Ga (I) and Ga (II). The Ga (I) atoms are bonded to four neighbouring O atoms in a tetrahedral arrangement whereas the Ga (II) atoms are in an octahedral arrangement bonded to six neighbouring O atoms. On the other hand, the O atoms have three distinct sites: O (I) and O (II) bonded to three Ga atoms and the O (III) is bonded to four Ga atoms. STHs in β - Ga_2O_3 are holes trapped by an O atom in an O(III) site with a Ga neighbour and or in O(I) site distributed among two O sites [6]. The blue emission is attributed to donor-acceptor pair (DAP) recombination. The donors are created by oxygen vacancies (VO), and the acceptors are created by gallium (VGa) or gallium–oxygen vacancy pairs (VGa – VO) [9].

The origin of the red emission is quite ambiguous, and the literature provides three plausible explanations involving doping by transition metals or rare earth metals [10-14, 19-21] or by

nitrogen [22, 23]. Figure 1b shows the CL spectra recorded in the region of 700 nm to provide more detail in the near IR region of the spectrum. The broad peak is seen for all the samples and order-sorting filters show that this is a combination of second order UV emission as well as real red emission. The narrow peaks seen around 690 nm, on the Fe doped sample (see black trace in Fig 1b) as well as on the other samples on increasing the beam current (data not shown here) are not due to second order effects. These narrow peaks resemble the R lines in ruby [24], and in order to understand more about the emission peaks around 690 nm, temperature dependent PL is performed.

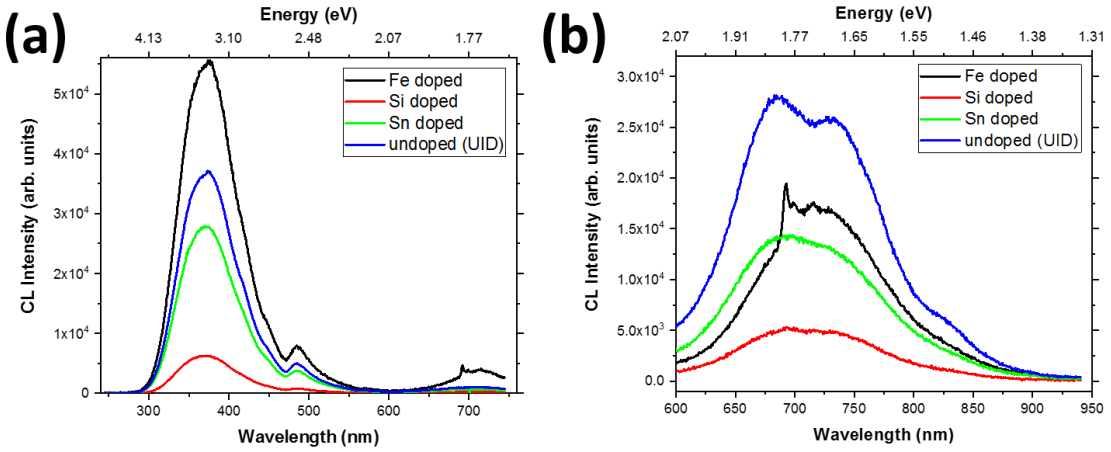

Figure 1: Room temperature CL spectra acquired at 5 keV (a) covering the whole visible range and (b) centre wavelength of 700 nm.

Figures 2a – 2c show PL performed at three different temperatures (290K, 125K and 10 K) for all four samples. The sharp lines are now clearly visible in all the samples except on the Sn-doped one, especially at low temperature. In literature, the R peaks at room temperature are at 695 nm (R1) and 688 nm (R2) [11]. At room temperature (290 K), the peak positions of the sharp lines for the UID and Fe doped sample are at 693.6 nm and 689.4 nm and thus matched to R1 and R2. The signal to noise is too low for the aforementioned peaks to be observed at RT for the Si doped sample. At an intermediate temperature of 125 K, the 689.4 nm and 693.6 nm peaks for the UID and Fe doped and Si doped samples have blue-shifted to 688.3 nm and

695.3 nm respectively. The sharp peak observed near 710 nm in Fig. 2 is the second-order line from the excitation source. The position of the second order line is used as a means of estimating the accuracy of the red emission peak positions, which have an offset of ≈ 1 nm. The two red emission peaks could not be observed on the Sn doped sample, which may well be due to the background shape of the spectra overwhelming the less intense red emission lines. In addition, Sn doping can affect the formation of the interstitial point defect complexes such as divacancy-interstitials, for example $2V_{Ga}^{1} - Sn_i$ complexes [25]. The high concentration of Sn may promote the formation of such defect complexes which act as compensating acceptor-like species that could inhibit the ionisation of rare-earth ions. This could explain the lower intensity or absence of red emission lines at room temperature in the Sn doped sample.

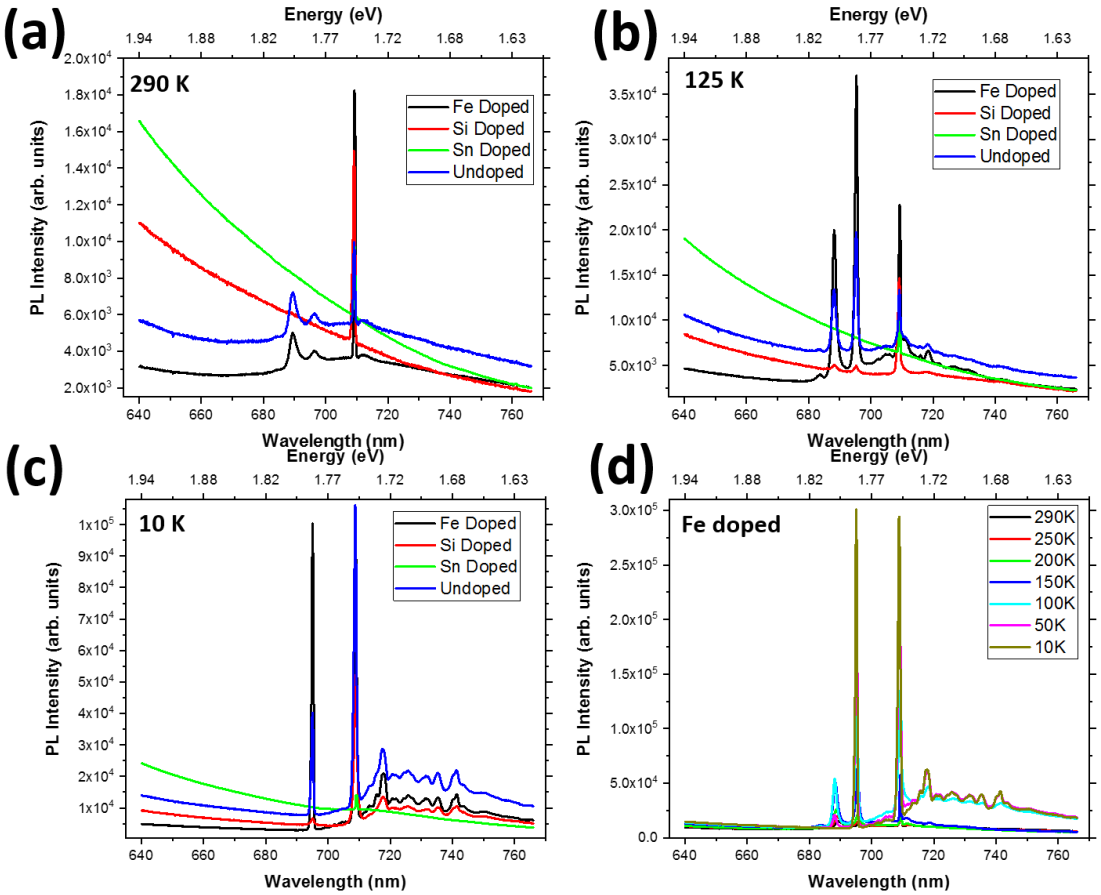

Figure 2: PL spectra at (a) 290 K, (b) 125 K, (c) 10 K for differently doped samples and (d) temperature dependent PL spectra from the Fe doped sample showing various red emission peaks. The sharp peak seen at 710 nm is the second order of the excitation laser.

In order to understand the peaks around 688 nm and 695 nm, temperature-dependent PL was performed for the Fe doped sample as shown in Fig, 2d. ~~If the excited electron state is within the same energy band, this excitation is referred as an intra-band transition. If the energy of the absorbed photon is greater than the energy of an allowable excitation between bands, then the excited electron will undergo an inter-band transition.~~ A number of sharp characteristic luminescence lines in the near-infrared region has been observed previously for GaAs doped with 3d transition-metal impurities , e.g. Cr, the origin being attributed to the zero-phonon intra-center transitions between the energy levels of the metal ions split by the crystal field of the host lattice [26]. These luminescence lines associated with different energy levels are very sensitive to the field surrounding the transition metal impurities [26]. Similarly, in GaN, transition metal ions such as Cr, Mn, Co and Fe can substitute Ga atoms and can cause sharp emission peaks due to intra-centre ionic transitions [27]. Recently, Polyakov et al [19] reported similar narrow emissions in β - Ga_2O_3 at 688.8 nm and 696.5 nm for Fe doped EFG samples, similar to the present work. The authors assigned these peaks to intra-centre transitions, most likely involving transition metal impurities. As they detect these emissions in samples doped with Fe, they associated them with the energy levels of $^4T_1 \rightarrow {}^6A_1$ intra-center transitions in Fe^{3+}. In the present work ,the narrow red emission peaks are also observed for UID as well as Si-doped samples. This raises an important question about the origin of these transition, which may well be due to other transition metal impurities such as Cr [10, 24]. It is well known that even very low concentrations, of the order of ppm, of Cr can result in strong luminescence [28, 29].

The Cr ion is known to emit two well-defined lines centered approximately at 1.78 eV (696.5 nm) and 1.80 eV (688.8 nm), the so-called R lines due to $^2E \rightarrow {}^4A_2$ electronic level transitions [11]. Figure 3 shows the analysis of the temperature dependence of the two red emission peaks. As shown in Fig. 3a, the 688 nm peak intensity increases on cooling from 290 K and reaches a

maximum intensity around 120 K after which it starts to decrease and eventually vanishes at 10 K. On the other hand, the 695 nm peak (see Fig 3b and 3d) increases in intensity on decreasing the temperature and reaches a maximum intensity at 10 K. Both peaks red shift in wavelength as the temperature increases (see Fig 3c). These trends agree with the R lines of Cr^{3+} in the Cr-doped Ga_2O_3 reported in the literature [30]. The broad luminescence band between 700 -750 nm with quite a few tiny peaks looks very similar to the PL results of Polyakov et al [19], however these peaks are also seen in the UID as well as the Si-doped sample. This broad red luminesence peak is due to the $^4T_2 \rightarrow {}^4A_2$ transition of Cr^{3+} in Ga_2O_3 [30], similar to the peaks seen at low temperature in the intentionally Cr-doped Ga_2O_3 samples reported in the work of Luchechko et al [11]. The high concetration of Fe in the Fe doped sample appears to enhance the CL intensity of R lines, and weak intensity is observed for the UID and Si doped samples. It is also possible for Cr to be dissolved in the Si lattice [31]. This may be the source for Cr ions in the Si doped HVPE sample, responsible for the R peaks. However, further work will be required to understand the role of Cr incorporation on the optical properties of Si doped Ga_2O_3 and on Ga_2O_3 grown on Si substrates.

It is also possible for Cr to be dissolved in the Si lattice [31] which could explain the occurance of the R peaks even in the Si doped sample grown by HVPE.

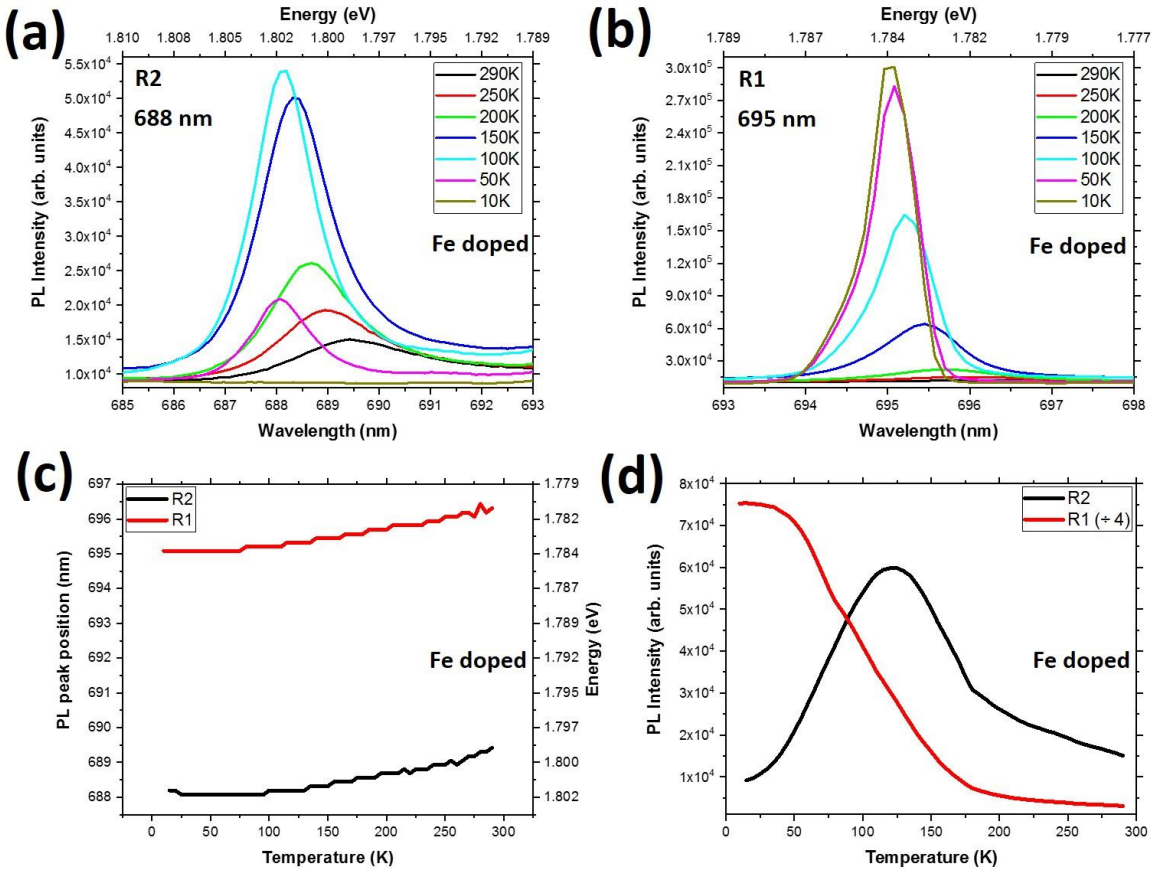

Figure 3: Temperature dependent PL spectra for the Fe-doped sample for the transitions at (a) 688 nm, (b) 695 nm, (c) peak positions and (d) peak intensities.

4. Conclusion

In summary, red emission from Si, Fe, Sn and unintentionally doped β - Ga_2O_3 grown by HVPE and EFG methods, respectively, were analysed using CL and PL spectroscopy. Sharp peaks are observed near 690 nm, and due to the higher concentration of Fe compared to the trace level of Cr in these samples, particularly in the Fe doped sample, these red emissions might be expected to be related to Fe^{3+} transitions. However, on monitoring the intensity of the peaks at ≈ 688 nm and 695 nm, at various temperatures, they resemble the R1 and R2 lines due to Cr^{3+} ions. Doping with Sn is seen to reduce the occurance of these R lines. The origin of the unintentional dopants on the samples in this work is likely to be the starting source material, although may also be from the crucibles used in the bulk growth methods for β - Ga_2O_3.

Acknowledgements

This work was supported by the EPSRC project "Quantitative non-destructive nanoscale characterisation of advanced materials" (EP/P015719/1) and from the University of Strathclyde Global Engagement Fund (grant no. 89266040). The data is available for download at https://dx.doi.org/... [to be completed in proofs].

Received: ((will be filled in by the editorial staff))
Revised: ((will be filled in by the editorial staff))
Published online: ((will be filled in by the editorial staff))

References

1. M. Higashiwaki, K. Sasaki, A. Kuramata, T. Masui, and S. Yamakoshi, Appl. Phys. Lett. **2012**, 100, 013504.
2. K. Tetzner et al., IEEE Electron Device Letters, **2019**, 40, 1503.
3. M. H. Wong et al., IEEE Electron Device Letters, **2020**, 41, 2.
4. A. S. Pratiyush, S. Krishnamoorthy, S. V. Solanke, Z. Xia, R. Muralidharan, S. Rajan, and D. N. Nathless, Appl. Phys. Lett., **2017**, 110, 221107.
5. S. J. Pearton, Jiancheng Yang, Patrick H. Cary, F. Ren, Jihyun Kim, Marko J. Tadjer, and Michael A. Mastro , Appl. Phys. Rev., **2018**, 5, 011301.
6. T. Gake, Y. Kumagai, and F. Oba, Phys. Rev. Mater., **2019**, 3, 44603.
7. A. Kyrtsos, M. Matsubara, and E. Bellotti, Appl. Phys. Lett., **2018**, 112, 3.
8. S. Yamaoka and M. Nakayama, Phys. Status Solidi C, **2016**, 13, 93.
9. L. Binet and D. Gourier, J. Phys. Chem. Solids, **1998**, 59, 1241.
10. R. Sun, Y. K. Ooi. P. T. Dickens, K. G. Lynn and M. A. Scarpulla, Appl. Phys. Lett., **2020**, 117, 052101.
11. A. Luchechko, V. Vasyltsiv, Y. Zhydachevskii, M. Kushlyk, S. Ubizskii and A. Suchocki, J. Phys. D: Appl. Phys., **2020**, 53, 354001.

12. H. H. Tippins, Phys. Rev., **1965**, 137, A865

13. M. D. McCluskey J. Appl. Phys., **2020**, 127, 101101.

14. M. Alonso-Orts et al. Phys. Rev. Appl. **2018**, 9, 064004.

15. A. Kuramata, K. Koshi, S.Watanabe, Y. Yamaoka,T. Masui and S. Yamakoshi, Jpn. J. Appl. Phys., **2016**, 55, 1202A2.

16. H. Murakami, K. Nomura, K. Goto, K. Sasaki, K. Kawara, Q. T. Thieu, R. Togashi, Y. Kumagai, M. Higashiwaki, A. Kuramata, S.Yamakoshi, B. Monemar and Akinori Koukitu Appl. Phys. Express, **2015**, 8, 015503.

17. P. R. Edwards, L. K. Jagadamma, J. Bruckbauer, C. Liu, P. Shields, D. Allsopp, T. Wang, and R. W. Martin, Microscopy and Microanalysis, **2012**, 18, 1212.

18. P. R. Edwards , K. P. O'Donnell, A. K. Singh, D. Cameron, K. Lorenz, M. Yamaga, J. H. Leach, M. J. Kappers and M. Bockowski, Materials, **2018**, 11, 1800.

19. A. Y. Polyakov, N. B. Smirnov, I. V. Schemerov, A. V. Chernykh, E. B. Yakimov, A. I. Kochkova, A. N. Tereshchenko and S. J. Pearton, J. Solid State Sci. Technol. **2019**, 8, Q3091.

20. T. Miyata et al. J. Luminescence, 2000, 87-89, 1183

21. P. Wellenius et al. J. Appl. Phys., **2010** 107, 103111

22. I. Hany, G. Yang ,C. E. Zhou ,C. Sun, K. Gundogdu, D. Seyitliyev, E. O. Danilov, F. N. Castellano, D. Sun, E. Vetter, Materials Letters, **2019**, 257, 126744.

23. Y.P. Song et al. Phys. Rev. B, **2004**, 69, 075304

24. A. Gonzaloa, E. Nogales, K. Lorenz, E.G. Víllora, K. Shimamura, J. Piqueras, B. Mendez, Journal of Luminescence, **2017**, 191, 56.

25. J. M. Johnson, Z. Chen, J. B. Varley, C. M. Jackson, E. Farzana, Z. Zhang, A. R. Arehart, H. Huang, A. Genc, S. A. Ringel, C. G. Van de Walle, D. A. Muller, J. Hwang, Physical Review X, **2019**, 9, 041027.

26. Y. Fujiwara, T. Nishino and Y. Hamakava, Jpn. J. Appl. Phys., **1982**, 21, 727

27. T. Zakrzewski and P. Bogusawski, Acta Phy. Pol. A, **2015**,127,321

28. B. Henderson and G. F. Imbusch, Optical Spectroscopy of Inorganic Solids, Clarendon, Oxford, 1989

29. M. Toth and M. R. Phillips, Appl. Phys. Lett., **1999**, 75, 3983.

30. E. Nogales, J. A. Garcia, B. Mendez and J Piqueras, J. Appl. Phys., **2007**, 101, 033517.

31. F. D. Heinz, F. Schindler, W. Warta, M. C. Schubert, Energy Procedia, **2013**, 38, 571.